1

Theory of thermal noise in optical mirrors

YURI LEVIN

1.1 Introduction

Mechanical and optical thermal noises play an important role in many precise optomechanical experiments, in which positions of test bodies are monitored by laser beams. Much of the initial experimental and theoretical research in this area was driven by the physics of gravitational-wave interferometers, where thermal fluctuations are expected to be the dominant source of noise in the frequency band between about 10 and 100 Hz (Harry *et al.*, 2002) (see Chapter 14). Recently, it has become clear that controlling thermal noise will be key in several other fields, notably in designing laser cavities with higher frequency stability (Numata *et al.*, 2004) (see Chapter 15), in reaching the quantum limit in macroscopic opto-mechanical experiments (Kippenberg and Vahala, 2008) (see Chapter 16), and in cavity QED experiments (Miller *et al.*, 2005) (see Chapter 17). In this chapter we review the statistical-mechanics formalism which is used to theoretically calculate mechanical and optical thermal noise. For completeness, we also add a discussion of another important limitation in mechanical measurements, the so-called Standard Quantum Limit.

1.2 Theory of mechanical thermal noise

The theory of time-dependent thermodynamical fluctuations has been extensively developed for the past century. One of the fundamental results in this field is the Fluctuation–Dissipation Theorem, which was originally formulated by Callen and Welton (1951). Callen and Welton's insight was that the intensity of random fluctuation in some *macroscopic* degree of freedom $\hat{x}$ of the thermodynamic system was proportional to the strength with which $\hat{x}$ was coupled to the *microscopic* degrees of freedom of the heat bath. Since the same coupling is responsible for damping of motion in $\hat{x}$, one obtains a proportionality relation between the microscopic thermal fluctuations of the quantity $\hat{x}$ and the damping coefficient for the macroscopic motion when $\hat{x}$ is driven externally. For optomechanical

Optical Coatings and Thermal Noise in Precision Measurement, eds. Gregory M. Harry, Timothy Bodiya and Riccardo DeSalvo. Published by Cambridge University Press.

experiments, $\hat{x}$ is typically an integrated quantity over a mirror surface. For example, in experiments with a test mass position readout by a laser, $\hat{x}$, is given by

$$\hat{x} = \int f(\vec{r})x(\vec{r}, t)d^2r. \tag{1.1}$$

Here $\vec{r}$ is the location of a point on the test-mass' mirror surface, and $x(r, t)$ is the displacement of the mirror along the direction of the laser beam at point $\vec{r}$ and time t. The form factor $f(\vec{r})$ depends on the laser beam profile and is proportional to the laser light intensity at the point $\vec{r}$ (Gillespie and Raab, 1995); it is usually normalized so that $\int f(\vec{r})d^2r = 1$.

The Fluctuation–Dissipation Theorem is then applied to the variable $\hat{x}$ by performing a mental experiment (Levin, 1998) consisting of the following three steps.

- Apply an oscillatory pressure $P(\vec{r}, t) = F_0 \cos(2\pi f t) f(\vec{r})$ to the face of the test mass. This is equivalent to driving the system with an external interaction Hamiltonian $H_{\rm int} = -F_0 \cos(2\pi f t)\hat{x}$.
- Work out the average power, $W_{\rm diss}$, dissipated in the test mass under the action of this oscillatory pressure.
- Compute the spectral density of fluctuations in $\hat{x}$ from

$$S_{\hat{x}}(f) = \frac{2k_{\rm B}T}{\pi^2 f^2}\frac{W_{\rm diss}}{F_0^2}, \tag{1.2}$$

  where $k_{\rm B}$ and T are the Boltzmann's constant and the temperature of the mirror respectively, and f is the frequency at which the spectral density is evaluated.

This method is straightforward to use. Once the dissipative processes are understood, the calculation reduces to a problem in elasticity theory (Levin, 1998; Bondu *et al.*, 1998) and, in the case of thermoelastic noise (see Section 1.3 and Chapter 9), time-dependent heat flow (Braginsky *et al.*, 1999; Liu and Thorne, 2000). For the important case of so-called structural damping (Saulson, 1990),

$$W_{\rm diss} = 2\pi f U_{\rm max}\phi(f), \tag{1.3}$$

where $U_{\rm max}$ is the energy of elastic deformation at a moment when the test mass is maximally contracted or extended under the action of the oscillatory pressure, and $\phi(f)$ is the loss angle characterising the dissipation. If the frequency band being measured is well below the normal modes of the test mass (as is often the case in gravitational wave detectors, see Chapter 14, frequency stabilization, see Chapter 15, and cavity QED experiments, see Chapter 17) one can assume constant, non-oscillating pressure $P(\vec{r}) = F_0 f(\vec{r})$ when evaluating $U_{\rm max}$. On the other hand, in many microscopic opto-mechanical experiments the detection frequencies are comparable to mechanical resonance frequencies, such as discussed in Chapter 16, and one needs to solve a time-dependent elasticity problem in order to find $U_{\rm max}$.

For the case of structural damping, and for frequencies much smaller than the mechanical resonant frequencies of the system, the thermal noise is approximately given by (Harry *et al.*, 2002)

$$S_{\hat{x}} = \frac{2k_B T}{\sqrt{\pi^3 f}} \frac{1-\sigma^2}{Y w_m} \left[\phi_{\text{substrate}}(f) + \frac{1}{\sqrt{\pi}} \frac{d}{w_m} A \phi_{\text{coating}}(f) \right], \tag{1.4}$$

where

$$A = \frac{Y'^2(1+\sigma)^2(1-2\sigma)^2 + Y^2(1+\sigma')^2(1-2\sigma')}{YY'(1-\sigma'^2)(1-\sigma^2)}. \tag{1.5}$$

Here Y and Y' are the Young's moduli of the substrate and coating, respectively, σ and σ' are their Poisson's ratios, d is the coating thickness, w_m is the radius where the field amplitude of the Gaussian laser beam is $1/e$, and $\phi_{\text{substrate}}$ and ϕ_{coating} are the loss angles of the substrate and the coating, respectively. This expression is valid when the beam size w_m is much smaller than the size of the mirror. When the latter approximation breaks down, one can find a series solution (Bondu *et al.*, 1998; Liu and Thorne, 2000) or an analytical solution for the coating thermal noise contribution (Somiya and Yamamoto, 2009) for axisymmetric configurations and use direct finite-element methods to calculate $U_{\max}$ for cases without the axial symmetry (Numata, 2003). See also Chapter 4.

Of the two contributions on the right-hand side of Equation 1.4, the one from the coating is projected to be the greater in most precision experiments. There are two essential reasons why the contribution from the coating is so large. The first one is geometrical: the sources of thermodynamically fluctuating random stress are spread out throughout the substrate and the coating, but the ones near the coating are closer to the surface and thus have greater effect on its displacement. This geometrical effect explains why the coating noise scales as $1/w_m^2$ while the structural substrate noise scales as $1/w_m$ (Levin, 1998). The second reason is that coating losses per volume are typically orders of magnitude greater than that of the substrates (see Chapters 4 and 7). Several practical proposals on how to reduce the unfavorable geometric factor have been investigated. The basic idea behind these proposals is to either increase the effective beam size by reconfiguring its shape towards a flat-top geometry or by working with higher-order cavity modes, see Chapter 13. Decreasing the mechanical loss of the coating is a great challenge in thermal noise research, and is discussed in Chapter 4. Other ideas for improving coating thermal noise are discussed in Chapters 6 and 8.

1.3 Theory of optical thermal noise

So far we have described mechanical thermal noise which appears due to small thermally driven random changes of the mirror's shape and results in random displacement of the mirror's surface. However, this description is not complete. Upon striking the mirror surface, the light penetrates several wavelengths into the coating, before being completely reflected.

The temperature within this skin layer of the coating is not constant, but fluctuates thermodynamically. These temperature fluctuations lead to random changes in the phase of the reflected light via two physical effects.

- The mirror surface shifts randomly due to the coating's thermal expansion. This is known as the coating thermoelastic noise (Braginsky and Vyatchanin, 2003a; Fejer *et al.*, 2004), and
- The optical pathlength inside the coating changes randomly, due to the temperature dependence of the coating's index of refraction. This is known as the thermorefractive noise (Braginsky *et al.*, 2000).

The thermorefractive and thermoelastic noises are typically anti-correlated, which reduces their impact on noise (Evans *et al.*, 2008; Gorodetsky, 2008) and are discussed in detail in Chapter 9 (see also Section 6.6). The theoretical evaluation of both of these noises involves calculating the spectra of thermal fluctuations of temperature-dependent quantities of the form

$$\delta\hat{T}(t) = \int q(\vec{r})\delta T(\vec{r}, t)d^3r. \tag{1.6}$$

Here $\delta T(\vec{r}, t)$ is the local fluctuation in temperature and $q(\vec{r})$ is the form factor proportional to the local intensity of light and the thermo-refractive coefficient $\partial n/\partial T$. A variation of the Fluctuation–Dissipation Theorem has been devised that allows one to calculate directly the spectral density $S_{\hat{T}}(f)$ (Levin, 2008). The calculation proceeds via a mental experiment similar to the one in the previous section. It consists of the following three steps.

- Periodically inject entropy into the medium, with the volume density of the entropy injection given by

$$\frac{\delta s(\vec{r})}{dV} = F_0 \cos(2\pi f t) q(\vec{r}), \tag{1.7}$$

  where F_0 is an arbitrarily small constant.
- Track all thermal relaxation processes in the system (e.g. the heat exchange between different parts of the system) which occur as a result of the periodic entropy injection. Calculate the total entropy production rate and hence the total dissipated power $W_{\rm diss}$ which occurs as a result of the thermal relaxation.
- Evaluate the spectral density of fluctuations in $\delta\hat{T}$ from

$$S_{\hat{x}}(f) = \frac{2k_{\rm B}T}{\pi^2 f^2}\frac{W_{\rm diss}}{F_0^2}. \tag{1.8}$$

This formalism was instrumental in the calculation of total thermo-optical coating noise (Evans *et al.*, 2008). It is likely to be useful for computing thermorefractive noise in experiments with non-trivial optical geometry, see Benthem and Levin (2009) for example.

1.4 Standard quantum limit

There is another source of noise which places an important limitation on opto-mechanical experiments. From the early days of quantum mechanics, it was clear that by precise measurement of a test mass' position one inevitably, and randomly, perturbs its momentum in accordance with the Heisenberg uncertainty relation $\Delta p \geq \hbar/(2\Delta x)$. Thus no matter which measurement device one uses, one inevitably introduces a *back-action* noise into the system; the higher the intrinsic precision of the measuring device, the greater the back-action noise. One can express this mathematically via the uncertainty relation (Braginsky and Khalili (1992))

$$S_x(f)S_F(f) - |S_{xF}(f)|^2 \geq \hbar^2/4, \tag{1.9}$$

where $S_x(f)$ is the spectral density of the intrinsic measurement noise, $S_F(f)$ is the spectral density of the back-action noise, and $S_{xF}(f)$ is the spectral density of the correlation between the measurement error and the back-action perturbation. For a vast majority of measuring devices the cross-correlation term S_{xF} is zero. Then the intrinsic and back-action noises, added in quadrature, enforce a limit on how precisely the position of a test-mass can be monitored. This is known as the standard quantum limit (SQL) (Braginsky and Khalili (1992) and references therein). For a free test body of mass m, the SQL is given by

$$S_x^{SQL}(f) = \frac{\hbar}{m(2\pi f)^2}. \tag{1.10}$$

As the coating noise is reduced due to technological progress, precision optical experiments will reach the SQL. However, the SQL is not a fundamental limit and can be overcome by using techniques of quantum optics which are capable of introducing correlations between a measurement error and a back-action perturbation, see Section 11.3 for discussion. Practical proposals exist on how to reach sensitivities below the SQL, see Kimble *et al.* (2001); Buonanno *et al.* (2001).

2

Coating technology

SHIUH CHAO

2.1 Introduction

The preparation and deposition of coatings can determine many of their basic properties. This chapter discusses the major technologies for creating thin film coatings, with an emphasis on those technologies most useful to precision measurement applications, as a baseline for the other chapters to expand on. There are many types of optical coatings, but we will be concerned with stacks of multi-layer thin films of dielectric materials with different refractive indices and thicknesses. Through optical interference effects, various optical functions can be achieved by properly selecting the materials and designing the layer thicknesses. Traditionally, the major application of coatings has been in imaging systems, including coatings on lenses, windows, and filters for purposes such as anti-reflection, band passing, polarization selection, etc. (Macleod, 2010; Baumeister, 2004a). With the advent of the laser and its diverse applications, high quality coatings for laser optics have become in high demand. Dielectric mirror coatings, which are often used in active or passive optical cavities, are particularly important.

The dielectric mirror is composed of a stack of thin films with pairs of alternating high and low refractive index materials. Conventionally, each layer has a quarter wave of optical thickness. Optical thickness is defined as $d_{\mathrm{opt}} = dn$, where d is the physical thickness of the layer, and n is the refractive index of the coating material. Given this, a quarter wave layer has $d_{\mathrm{opt}}/\lambda = 1/4$, where λ is the wavelength of light for which the coating is designed. Reflectance of the mirror increases with the increasing number of pairs and the increasing refractive index difference between the pair materials in general. For a quarter wave stack, the reflectivity in air at normal incidence can be found from

$$r = \frac{1 - n_s\,(n_1/n_2)^{2\mathrm{p}}}{1 + n_s\,(n_1/n_2)^{2\mathrm{p}}}, \tag{2.1}$$

where r is the reflected field amplitude, n_s is the refractive index of the substrate, n_1 and n_2 are the refractive indices of the two coating materials, and p is the number of pairs of a high and low index material in the coating.

Optical Coatings and Thermal Noise in Precision Measurement, eds. Gregory M. Harry, Timothy Bodiya and Riccardo DeSalvo. Published by Cambridge University Press.

High-end applications for the mirror coatings all require that the coatings have low optical losses, i.e. low absorption (see Chapter 10) and low scattering (see Chapter 11). In a ring laser gyroscope, for example, extremely low backscattering (typically less than a few ppm) in the mirror is required in order to avoid frequency lock-in so that low rotation rates can be detected (Kalb, 1986). Furthermore, some additional applications now require low thermal noise (see Chapter 5, 14–17). Beginning in the 1970s, researchers also intensively studied laser induced damage stemming from optical coating losses in high energy laser applications, such as laser ignition fusion (Stolz and Taylor, 1992).

In addition to low optical losses, narrow-band thin film filters composed of multiples of half-wavelength thick films in between quarter wave stacks are required to have a narrow pass-band width as low as sub-nm and to be environmentally stable while operating in the field. These types of filters are critical for dense wavelength division multiplexing (DWDM) technology in optical communication. These criteria impose high thickness control and environmental stability requirements on the coatings (Takashashi, 1995). The stringent requirements of high-end applications drove rapid progress in optical coating technology since the 1970s. This chapter introduces coating methods, coating processes, and thin film materials used in high-end coating technologies with the purpose of stimulating further research and development activities on coatings for precision measurement.

2.2 Coating methods

Various coating methods have been developed to provide films with desired qualities such as good optical characteristics, uniformity, precise thickness control, absence of stress and defects, strong adhesion, ease of fabrication, large throughput, and low fabrication cost. Among the many factors that affect the film qualities, one of fundamental importance is the kinetic energy of the coating material atoms when impinging on the substrate prior to condensation. Upon arriving at the substrate surface, the atoms need a sufficient amount of energy to overcome the activation energy of various mechanisms to reach proper sites for nucleation and growth. This will allow for a close-packed structure and good adhesion to the substrate and the neighboring layer (Neugebauer, 1970; Ohring, 2002). In the following sections, we shall introduce different coating methods, with emphasis on energetics.

2.2.1 Thermal evaporation

Thermal evaporation is the most commonly used coating method. Source material is heated by resistance heating or by electron beam bombardment to either the sublimation or melting point. The evaporants then condense on the substrate to form a thin film. Most compounds do not evaporate to form films that have the same composition as the source material, and various means for reactive evaporation or multiple single element source co-evaporations need to be implemented to insure the correct stoichiometry for the films. The average kinetic energy of the evaporant when impinging the substrate is the thermal energy at the melting

point, typically of the order of 10^{-1} eV. This is a relatively low energy and therefore the atoms have difficulty migrating on the substrate surface and forming a dense, less porous film. The film is therefore susceptible to moisture when exposed to the atmosphere, which can lead to weak adhesion to the substrate and a low refractive index.

There are many methods to increase the energy of the evaporant (Vossen and Kern, 1978); substrate heating, DC or RF biasing of the substrate, and more recently employed, ion beam assisted deposition (IBAD). IBAD uses a low energy and high current broad ion beam to bombard the substrate, assisting the film formation with denser packing and enhanced oxidation/nitridation when the ion beam contains oxygen/nitrogen ions for deposition of oxide/nitride films (Green *et al.*, 1989). Since the evaporation process is performed in a high vacuum, typically 10^{-6} Torr, the mean free path of the evaporant is a few tens of meters. The evaporant distribution is nearly Lambertian; the evaporant has a large field of view. In addition, a high evaporation rate is easy to achieve by increasing the temperature of the melt with electron beam bombardment. Therefore, high throughput deposition can be realized in a large box coater that can accommodate a large quantity of substrates positioned in planetary rotation dome-shaped holders. Currently, electron beam evaporation with the IBAD method is the primary coating technique for large quantities of fairly good quality batched optical coatings.

2.2.2 Glow discharge sputtering

The glow discharge sputter deposition technique dates back to the nineteenth century, when deposits of cathode material were observed in DC glow discharge environments. In a straightforward planar DC glow discharge, the target serves as the cathode and the substrate serves as the anode. At the state of "abnormal glow" for sputtering, most of the discharge voltage falls in the Crookes dark space adjacent to the cathode. The positive ions in the neighboring negative glow region gain kinetic energy, typically a few hundreds to 1000 eV, from the cathode fall and bombard the cathode to sputter off the cathode atoms. The sputtered atoms have kinetic energy of a few tens of eV (see Section 2.2.3). Initiating voltage for the glow discharge varies with the product of the gas pressure and the electrode separation with a deep minimum according to Paschen's law, which limits the operating gas pressure and electrode separation. A typical value for electrode separation is a few cm and for gas pressure is in the range of 10^{-2} Torr. This is a relatively high pressure and the mean free path of the sputtered atoms is therefore short. The consequence is that the kinetic energy of the sputtered atoms tends to be thermalized through multiple collisions on the way to the substrate. A typical value for the kinetic energy of the sputtered atoms when impinging the substrate is on the order of 1 eV, which is lower than that in ion beam sputtering (see Section 2.2.3) but about ten times higher than that of the evaporation process. Therefore, film qualities of adhesion, density, refractive index, and moisture susceptibility are generally better than that of the films deposited by thermal evaporation. Nevertheless, since the substrate is immersed in plasma during deposition, the films may be subjected to UV damage and re-sputter.

Both triode sputter, in which a thermionic electrode is added to the diode, and magnetron sputter, in which a magnetic field is applied to confine the plasma, can increase the collision probability between the electron and the gas atoms to enhance the plasma generation efficiency. This allows lower gas pressure, lower power or larger electrode distance to be accommodated. When the sputter target is an electrical insulator, a radio frequency (13.56 MHz) source is applied. The heavier ion is less responsive to the high frequency RF field than the electrons in the plasma, establishing a self-bias at the target for sputtering. One advantage of glow discharge sputtering is that very large targets can be used, such that large substrates, e.g. architectural window glass, solar panels, display panels, plastic rolls, etc, can be coated in a load-lock conveyer-fed coater or a web-coater for uninterrupted continuous large volume coating operations.

2.2.3 Ion beam sputter deposition (IBSD)

Most of the optical coatings for high-end applications mentioned in Section 2.1 are fabricated by the ion beam sputter deposition method (IBSD). The ion beam source was originally used as a spacecraft thruster, only later was it applied to ion etching and thin film deposition. In recent years, the focused ion beam (FIB) technique has been developed for semiconductor device fabrication, diagnosis, and nano-patterning (Joe *et al.*, 2009). Wei and Louderback (1979) first used the IBSD technique to sputter deposit mirrors for a ring laser gyroscope, obtaining unprecedented quality. The technique then became the major coating method for high quality optical coatings.

The schematic of an IBSD apparatus with a conventional Kaufman type ion source, i.e. hot filament with extracting grids, is shown in Figure 2.1. High density plasma is generated in the discharge chamber and ion beamlets are extracted, accelerated through the apertures in the grids to form a broad ion beam, and hit the target. The target atoms are, then, sputtered off and condense on the substrate to form the films. Several targets can be attached to the rotatable target holder for coating multi-layers. Planetary rotation fixtures can be used to obtain films with uniform thickness distribution.

Ion source

The conventional ion beam generation method is the use of the Kaufman type ion source. Referring to Figure 2.1, electrons emitted from the hot cathode through thermionic emission collide with gas atoms, typically argon gas, to produce positive ions and electrons. The ionization energy for argon is 15.76 eV, and around a 40 V voltage difference between the cathode and the anode with a few mTorr of gas pressure is sufficient to sustain the plasma. The anode is typically held at a voltage from 500–1000 V above ground, and the plasma potential is nearly the same value. The target is held at the ground potential. The average kinetic energy of the ions is therefore 500–1000 eV when hitting the target. The screen grid is held to roughly the anode potential and the accelerator grid is negatively biased to about −100 V. Both grids are precisely aligned to each other so that ion beamlets are extracted

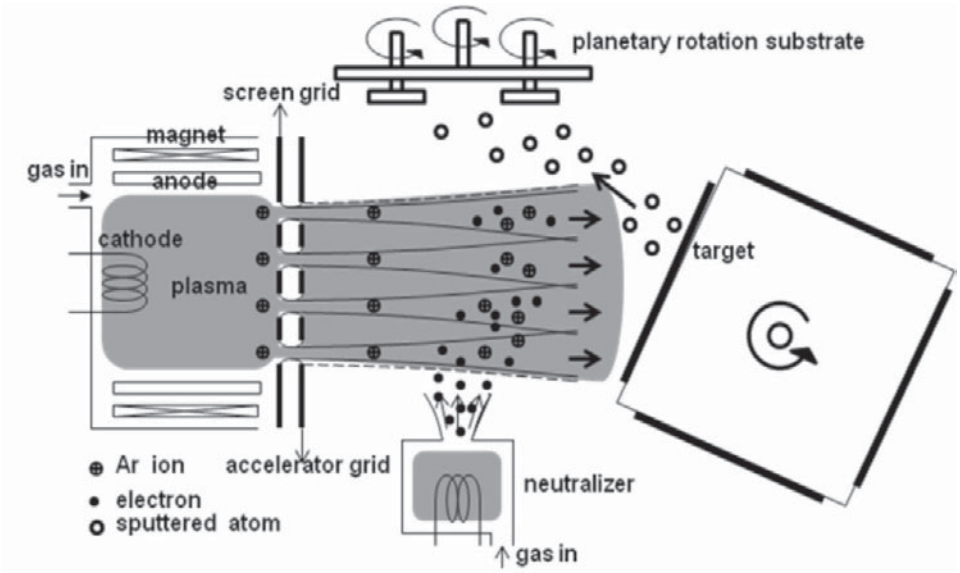

Figure 2.1 Schematics of an ion beam sputter setup.

and accelerated through the apertures. Factors such as grid separation, aperture size, grid curvature, applied voltage, plasma density, etc, affect the beam shape, beam divergence and the current density. Thorough reviews for the physics and characteristics of the Kaufman ion source are given in Kaufman *et al.* (1982); Harper *et al.* (1982). The grids are made of graphite or molybdenum, which have higher resistance to ion bombardment within the aperture. A plasma bridge neutralizer, usually a thermionic cathode or a hollow cathode which emits electrons to neutralize the ion beam for sputtering the insulator targets, is positioned aside the beam path. For depositing oxide films, oxygen gas with pressure around 10^{-4}–10^{-5} Torr is fed into the sputter chamber to oxidize the films during deposition. A second ion source is sometimes used to bombard the substrate for ion beam assisted sputter deposition. The second ion source is generally low energy and high current so that the film will not be re-sputtered and yet sufficient energy can be added to assist film growth. The second ion beam could be an oxygen ion beam or a mixture of oxygen and argon to enhance the oxidation for the oxide film.

A major drawback to the hot filament ion source is the frequent filament maintenance required. The filament might break down during long-term continuous deposition (e.g. coating for DWDM filters, the filament is subjected to ion bombardment and the ion beam may become contaminated). Two other advanced plasma generation methods have been developed to avoid hot filament issues; radio frequency (RF) and electron cyclotron resonance (ECR) plasma generation. RF power, with a frequency of 13.56 MHz, is fed into the discharge chamber, usually by inductive coupling, i.e. through a solenoid coil or a flat spiral coil that is embedded in a dielectric shield. Electrons oscillate in the RF field